Applied Catalysis B: Environmental 183 (2016) 47–52

Contents lists available at ScienceDirect

Applied Catalysis B: Environmental

journal homepage: www.elsevier.com/locate/apcatb

Self-assembly of CPO-27-Mg/TiO_2 nanocomposite with enhanced performance for photocatalytic CO_2 reduction

Mengtao Wang, Dengke Wang, Zhaohui Li*

Research Institute of Photocatalysis, State Key Laboratory of Photocatalysis on Energy and Environment, College of Chemistry, Fuzhou University, Fuzhou 350002, PR China

ARTICLE INFO

Article history:
Received 30 August 2015
Received in revised form 17 October 2015
Accepted 18 October 2015
Available online 21 October 2015

Keywords:
Photocatalysis
CO_2 reduction
Metal-organic framework
Titanium dioxide

ABSTRACT

CPO-27-Mg (also referred to as Mg_2(DOBDC), DOBDC = 2,5-dioxido-1,4-benzenedicarboxylate), a Mg^{2+} based metal-organic framework which shows the highest CO_2 uptake among the already reported MOF materials, was chosen to combine with TiO_2 to form CPO-27-Mg/TiO_2 nanocomposite via a hydrothermal self-assembly method. The as-obtained CPO-27-Mg/TiO_2 nanocomposite is composed of TiO_2 nanospheres on the spindle-shaped CPO-27-Mg microcrystal. Intimate contact between CPO-27-Mg and TiO_2 nanospheres exists due to the coordination between the carboxylate groups in DOBDC and Ti^{4+} in TiO_2. The as-obtained CPO-27-Mg/TiO_2 nanocomposite exhibited enhanced performance for the photocatalytic CO_2 reduction to form CO and CH_4 due to its high adsorption capacity toward CO_2 and the existence of open alkaline metal sites in CPO-27-Mg. By incorporating MOFs with open alkaline metal center into TiO_2, the reduction of H_2O to H_2, a competitive reaction to photocatalytic CO_2 reduction, was totally inhibited. This study highlights the promising prospect of incorporating MOFs with open alkaline metal sites into semiconductors for artificial CO_2 photo-conversion.

1. Introduction

The utilization of solar energy for the conversion of CO_2 into valuable chemical fuels is one of the most attractive routes to alleviate the energy crisis and global warming [1,2]. So far, various photocatalysts, including inorganic semiconductors [3,4], metal-incorporated zeolites [5], and homogeneous transition-metal complexes [6], have been investigated for their performances in photocatalytic conversion of CO_2. Although TiO_2 has been well demonstrated to be a promising material in photocatalytic degradation of all kinds of organic contaminants [7], its photocatalytic activity for CO_2 reduction is limited, partially due to its poor adsorption capability toward CO_2. The combination of TiO_2 with materials with remarkable CO_2 adsorption capacity, like zeolites or other meso-porous materials, has been found to be a promising method to enhance its photocatalytic performance for CO_2 reduction [8,9].

Metal-organic frameworks (MOFs) are an intriguing family of crystalline micro-mesoporous hybrid materials constructed from metal clusters interconnected by multitopic organic ligands with an extended 3D network. Their inherent high specific surface areas, tunable and well-defined nanometer-scale cavities, and tunable chemistry have enabled them to show a variety of promising applications in many areas, such as gas storage [10,11] and separation [12–14], luminescence [15,16], molecular recognition [17], drug delivery [17,18], heterogeneous catalysis and photocatalysis [19–21]. Due to their excellent adsorption capacity toward CO_2 [22,23], recently MOFs have been used as photocatalysts for CO_2 reduction [24–26]. Besides being directly used as photocatalysts, MOFs can also form composites with inorganic semiconductor photocatalysts for efficient CO_2 reduction taking advantage of its superior adsorption toward CO_2. A couple of studies reported in this field did show that the incorporating MOFs into semiconductor photocatalysts would be a promising strategy for promoting the photocatalytic CO_2 reduction [27,28].

Herein we report the construction of CPO-27-Mg/TiO_2 composite via an in situ hydrothermal method and its performance for photocatalytic CO_2 reduction. CPO-27-Mg (also referred to as Mg_2(DOBDC), DOBDC = 2, 5-dioxido-1,4-benzenedicarboxylate) is characterized by a honeycomb-like structure with large one-dimensional pores of ~11–12 Å diameters [29]. Why CPO-27-Mg was chosen to combine with TiO_2 lies in that it not only shows the highest CO_2 uptake (about 35.2 wt%) among the already reported MOF materials, but also it possess a high concentration of open alkaline metal sites (Mg^{2+}) in its structure, which is believed to be beneficial for CO_2 activation [30,31]. Our studies revealed that CPO-27-Mg/TiO_2 nanocomposite exhibited enhanced performance

* Corresponding author. Fax.: +86 059183779260.
E-mail addresses: zhaohuili1969@yahoo.com, zhaohuili@fzu.edu.cn (Z. Li).

http://dx.doi.org/10.1016/j.apcatb.2015.10.037
0926-3373/

for the photocatalytic CO_2 reduction to form CO and CH_4 due to its high adsorption capacity toward CO_2 and the existence of open alkaline metal sites in CPO-27-Mg.

2. Experimental

2.1. Syntheses

All the reagents are analytical grade and used without further purifications. TiO_2 nanospheres were synthesized according to our previously reported method [32]. CPO-27-Mg/TiO_2 composite was synthesized via a mixed solvo-thermal method from H_4DOBDC and $Mg(NO_3)_2{\cdot}6H_2O$ in the presence of the as-prepared TiO_2 nanospheres following the procedures previously reported [33]. H_4DOBDC (0.121 g, 0.61 mmol) was dissolved in THF (18 ml) in the 50 ml Teflon inlet of autoclave and NaOH (2.5 ml, 1 mol L^{-1}) was added to this solution under constant stirring. The as-prepared TiO_2 nanospheres (0.16 g, 2 mmol) and $Mg(NO_3)_2{\cdot}6H_2O$ (0.312 g, 1.21 mmol) in 5 ml de-ionized water was added to the above mentioned solution. After 30 min vigorous stirring, the autoclave was sealed and reacted at 110 °C for 3days. The as-obtained product was collected by filtration, washed thoroughly with methanol and dried at 60 °C in vacuum. For comparison, SBA-15/TiO_2 was prepared from $TiOSO_4$ and SBA-15 via a hydrothermal method. ZIF-8/TiO_2 was prepared from 2-methylimidazole, $Zn(NO_3)_2{\cdot}6H_2O$ and TiO_2 nanosphere.

2.2. Characterizations

Powder X-ray diffraction (XRD) data were collected using a Bruker D8 Advance X-ray diffractometer (Cu Kα irradiations). The morphology of the product was characterized by a field emission scanning electron microscopy (SEM, Hitachi-SU-8000). The transmission electron microscopy (TEM) and high-resolution transmission electron microscopy (HRTEM) images were measured by a JEOL model JEM 2010 EX instrument at an accelerating voltage of 200 kV. Thermo-gravimetric analysis (TGA) of the sample was performed on a Pyris Diamond TG/DTA thermo-gravimetric analyzer (PerkinElmer Thermal Analysis). Samples were heated under an air atmosphere from 30 to 800 °C at 5 °C/min. BET surface area and the CO_2 adsorption were carried out on an ASAP2020 M apparatus (Micromeritics Instrument Corp., USA). After the samples were degassed in vacuum at 200 °C for 24 h, the nitrogen adsorption and desorption isotherms were measured at −196 °C, and CO_2 adsorption isotherms were measured at 0 °C. UV–visible absorption spectra (UV-DRS) of the powders were obtained for the dry-pressed disk samples using a Cary 500 Scan Spectrophotometer (Varian, USA). $BaSO_4$ was used as a reflectance standard in the UV–visible diffuse reflectance experiment.

2.3. Photocatalytic conversion of CO_2

Before the photocatalytic CO_2 reduction, the photocatalysts were treated under vacuum at 200 °C to remove the solvent. The photocatalytic reactions were performed in a 10 ml quartz schlenk tube pre-saturated with CO_2 atmosphere in the presence of saturated water vapor. 10 mg of photocatalyst was evacuated and purged with CO_2. Four 4 W UV lamps with a wavelength centered at 365 nm were used as illuminating source. The amounts of CH_4, H_2 and O_2 evolved after reaction were analyzed by using a GC-TCD–FID (Shimadzu GC-2014) with a TDX-01 packed column. CO was converted to CH_4 by a methanation reactor and then analyzed by using the FID detector of GC.

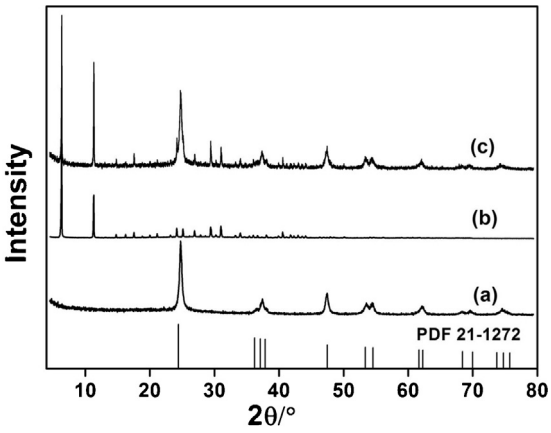

Fig. 1. Powder X-ray diffraction patterns of (a) TiO_2 spheres, (b) pure CPO-27-Mg, and (c) CPO-27-Mg/ TiO_2 nanocomposite.

3. Results and discussion

Anatase TiO_2 nanospheres were prepared from $TiOSO_4$ and was used for the in-situ construction of the CPO-27-Mg/TiO_2 composite by reacting with Mg $(NO_3)_2$ and H_4DOBDC hydrothermally. The XRD pattern of the as-prepared product show diffraction peaks attributable to CPO-27-Mg, in addition to those corresponding to anatase TiO_2 (Fig. 1). The SEM image shows that spindle-shaped microcrystals in a dimension of about 10 μm were densely cover with nanospheres in a size of 300–500 nm (Fig. 2a). By comparing with pure CPO-27-Mg and TiO_2 nanospheres, it is obvious that the formation of the composite does not influence their original morphology (Supporting Figs. S1 and S2). The TEM image of the CPO-27-Mg/TiO_2 composite exhibits the close adherence of the TiO_2 nanospheres on the spindle-shaped CPO-27-Mg microcrystal. A clear lattice fringe of 0.352 nm observed in the high-resolution TEM (HRTEM) image can be assigned to the inter-planar distance between adjacent (1 0 1) crystallographic planes of anatase TiO_2 (Fig. 2b). TG analysis was carried out to quantify the weight ratio of CPO-27-Mg in the composite. The TG of the composite exhibits three weight losses, among which the third weight loss in the range of 420–510 °C can be assigned to the decomposition of the framework of CPO-27-Mg (Supporting Fig. S3) [33]. Based on the TG result, the amount of CPO-27-Mg in the composite was determined to be 39.3 wt%. As expected, the BET specific surface area of the as-prepared CPO-27-Mg/TiO_2 (416.81 $m^2\ g^{-1}$) is much higher than that of pure TiO_2 nanospheres (92.35 $m^2\ g^{-1}$) (Supporting Fig. S4). Besides this, the incorporation of CPO-27-Mg also leads to a significant increase of the adsorption capability toward CO_2 from the original 19.94 $cm^3\ g^{-1}$ for TiO_2 to 106.59 $cm^3\ g^{-1}$ for the composite (Fig. 3). It is believed that the enhancement of the adsorption capability toward CO_2 may promote its photocatalytic performance for CO_2 reduction.

The UV/visible DRS spectra of the as-obtained CPO-27-Mg/TiO_2 composite shows two main absorption in the range of 200–380 nm and 380–460 nm together with a shoulder peak extending to 600 nm, in accordance with its brown yellow color (Fig. 4). By comparing it with that of pure CPO-27-Mg and TiO_2 nanospheres, it is obvious that the first UV absorption can be ascribed to the overlap of the band gap absorption of anatase TiO_2 and the LMCT of O to Mg in an octahedral coordination environment, while the second absorption band in the range of 380–460 nm can be attributed to the absorption by the ligand DOBDC in CPO-27-Mg. The shoulder absorption extending to 600 nm, which is not observed in either the UV–visible spectra of pure TiO_2 or CPO-27-Mg, should be attributed to the interaction between the O in DOBDC ligand and Ti in anatase

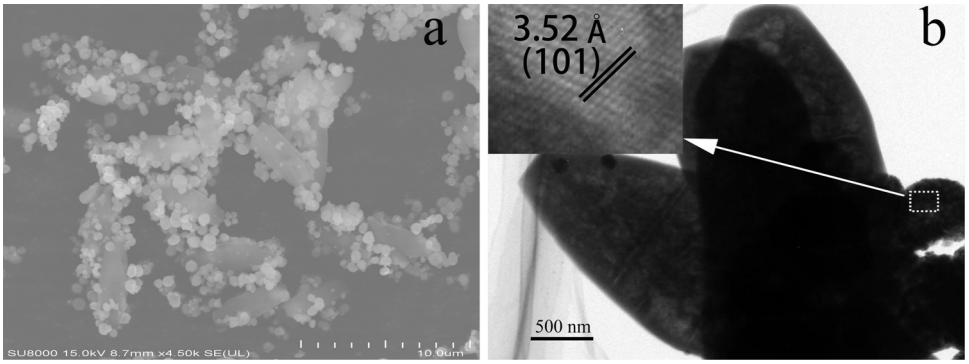

Fig. 2. SEM images (a) and TEM images (b) of CPO-27-Mg/TiO_2 nanocomposite (inset HRTEM image).

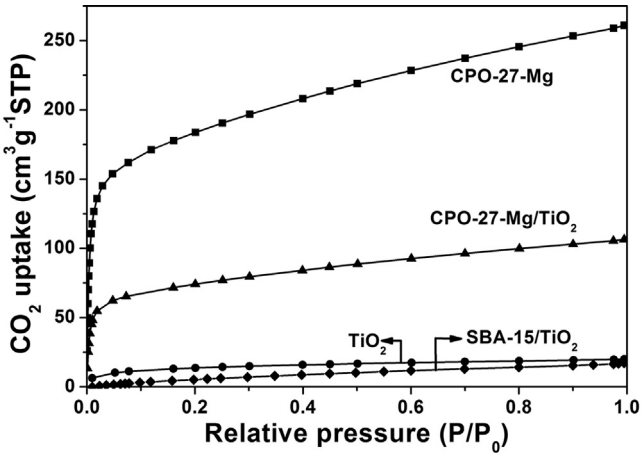

Fig. 3. (a) CO_2 adsorption behaviors over CPO-27-Mg, TiO_2 spheres, CPO-27-Mg/TiO_2 and SBA-15/TiO_2 nanocomposite.

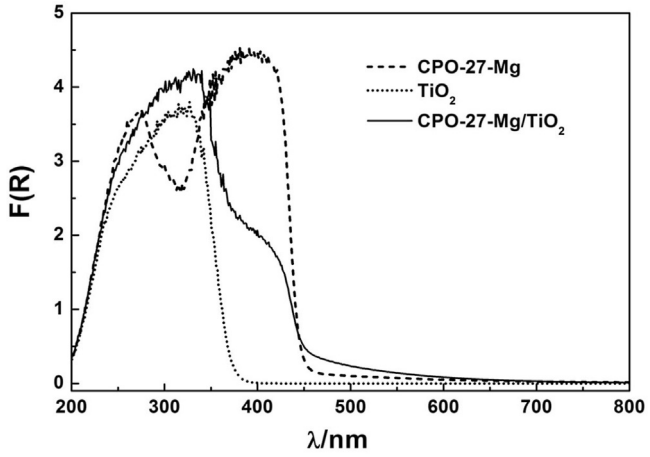

Fig. 4. UV–visible adsorption spectra of CPO-27-Mg/TiO_2 nanocomposite, CPO-27-Mg and TiO_2 nanospheres.

TiO_2, a confirmation that there exists intimate contact between CPO-27-Mg and TiO_2 nanospheres.

To investigate how the morphology of the CPO-27-Mg/TiO_2 nanocomposite was formed, the time-dependent experiments were carried out and the SEM images of the products obtained in different reaction time were shown in Supporting Fig. S5. The SEM image of the product obtained after 0.5 h reaction shows that the surface of TiO_2 nanospheres were covered with small particles. When the reaction time was prolonged to 10 h, the SEM image of the product shows the deposition of TiO_2 nanospheres on the spindle-like CPO-27-Mg with a length of 6 μm. With the reaction time prolonged to 72 h, the length of the spindle was enlarged to 12 μm. We believed that the formation of the CPO-27-Mg/TiO_2 nanocomposites with TiO_2 nanospheres on the spindle-shaped CPO-27-Mg microcrystal is possibly due to the unique structure of CPO-27-Mg. CPO-27-Mg is a Mg^{2+} based metal-organic framework with unique 1D hexagonal channels and a special 1D threefold helical chains in its structure, which makes it prefer to growth longitudinally, as well evidenced in previous studies.

Based on the time-dependent reactions, the formation of CPO-27-Mg/TiO_2 composite between CPO-27-Mg and TiO_2 is illustrated in Scheme 1. First, the carboxylate and hydroxyl groups in DOBDC can coordinate with Ti^{4+} in anatase TiO_2 nanospheres. Then the nuclei of CPO-27-Mg can form on the surface of TiO_2 through the coordination between Mg^{2+} and DOBDC under an appropriate solvothermal treatment. Due to the growth habit of CPO-27-Mg, these nanoparticles on TiO_2 nanospheres can self-assembly to form spindle-shape CPO-27-Mg with TiO_2 deposited on its surface. With prolonged reaction time, the size of the CPO-27-Mg on anatase TiO_2 grow larger. Such an in-situ formation mechanism was previously observed in the formation of Zn-MOF-5/TiO_2 [34].

To study the influence of CPO-27-Mg on the photocatalytic performance of TiO_2, the photocatalytic CO_2 reduction were carried out over CPO-27-Mg/TiO_2 in a CO_2 atmosphere with water vapor. Although CPO-27-Mg/TiO_2 composite shows absorption in the visible region, no reduction product was observed when it was irradiated with visible light. When CPO-27-Mg/TiO_2 was irradiated with 365 nm UV light, 40.9 μmol g^{-1} of CO and 23.5 μmol g^{-1} of CH_4 as well as 62.9 μmol g^{-1} of O_2 were detected after 10 h irradiations (Fig. 5a). On the contrary, only 22.5 μmol g^{-1} of CO

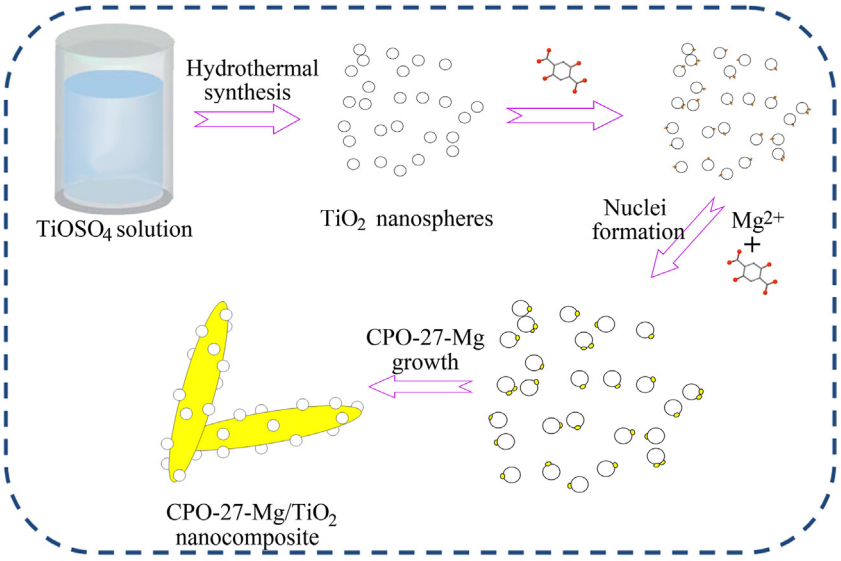

Scheme 1. Schematic illustration of the formation of CPO-27-Mg/TiO_2 nanocomposite.

and 13.7 μmol g^{-1} of CH_4 were produced over irradiated TiO_2 nanospheres. In addition to the products from CO_2 reduction, 11.3 μmol g^{-1} of H_2 was also produced over pure TiO_2. Both the amount of CO and CH_4 produced over CPO-27-Mg/TiO_2 is much higher than that over the pure TiO_2. Moreover, the incorporation of CPO-27-Mg into TiO_2 can totally inhibit the reduction of H_2O to form H_2, which is a competitive reaction of the CO_2 reduction.

For comparison, the photocatalytic activity for CO_2 reduction over a physical mixture of TiO_2 and CPO-27-Mg (with the ratio of TiO_2 to CPO-27-Mg in 6:4) was also studied and was compared with that of the CPO-27-Mg/TiO_2 composite. It was found that 8.5 μmol g^{-1} of H_2, 18.9 μmol g^{-1} of CO and 7.1 μmol g^{-1} of CH_4 were produced over a physical mixture of TiO_2 and CPO-27-Mg under otherwise similar condition. Both the amount of CO and CH_4 produced over the mixture is much lower than that over CPO-27-Mg/TiO_2 nanocomposite (40.9 μmol g^{-1} of CO and 23.5 μmol g^{-1} of CH_4), indicating the strong interaction between TiO_2 and CPO-27-Mg formed via the in situ hydrothermal method is beneficial for the photocatalytic CO_2 reduction.

Usually the surface area of the photocatalyst plays an important role in the photocatalytic reaction. To differentiate the influence of the surface area on the photocatalytic CO_2 reduction, the photocatalytic CO_2 reduction over SBA-15/TiO_2, a photocatalyst with comparable BET specific surface area as that of CPO-27-Mg/TiO_2, was studied. It was found that 36.9 μmol g^{-1} of CO was produced over SBA-15/TiO_2 after irradiated for 10 h. The amount of CO_2 reduced products over SBA-15/TiO_2 (36.9 μmol g^{-1} of CO) is much lower than that over CPO-27-Mg/TiO_2 (40.9 μmol g^{-1} of CO and 23.5 μmol g^{-1} of CH_4), indicating that the increase of the surface area is not pivotal in the enhancement of the photocatalytic CO_2 reduction over CPO-27-Mg.

Since the adsorption capacity toward CO_2 plays an important role for photocatalytic CO_2 reduction, the photocatalytic activity for CO_2 reduction over ZIF-8/TiO_2, a photocatalyst with comparable CO_2 adsorption as that of CPO-27-Mg/TiO_2, was also investigated under otherwise similar condition. It was found that 29.8 μmol g^{-1} of CO and 14.7 μmol g^{-1} of CH_4 were produced over ZIF-8/TiO_2 after 10 h irradiations. Although these values are a little higher than those over pure TiO_2 (22.5 μmol g^{-1} of CO and 13.7 μmol g^{-1} of CH_4), they are much lower than those over CPO-27-Mg/TiO_2 (40.9 μmol g^{-1} of CO and 23.5 μmol g^{-1} of CH_4). This result clearly indicates that the open alkaline metal sites in CPO-27-Mg also play an important role in the photocatalytic CO_2 reduction.

Based on the above controlled experiments, the superior photocatalytic activity for CO_2 reduction observed over CPO-27-Mg/TiO_2 can be attributed to the following factors. First, CPO-27-Mg/TiO_2 composites show superior adsorption capacity toward CO_2. Second, the existence of the open alkaline metal sites in CPO-27-Mg may facilitate the photocatalytic CO_2 reduction since previous study showed that the alkaline environment in the reaction system can lower the reaction barrier for CO_2 reduction [35,36].

By incorporating CPO-27-Mg into TiO_2, the reduction of H_2O to H_2 was completely inhibited in the process of photocatalytic CO_2 reduction. The change of the product selectivity may be related to the alkaline environment caused by the incorporation of CPO-27-Mg. It is generally known that the photocatalytic CO_2 reduction is a competing reaction of the photocatalytic hydrogen evolution. The presence of the alkaline metal site in CPO-27-Mg is beneficial for the CO_2 reduction owing to the lower reaction barrier for CO_2 reduction in the alkaline environment. On the contrary, the release of H^+, which is an important step in the photocatalytic hydrogen evolution, is suppressed in an alkaline environment [37,38].

The effect of CPO-27-Mg amount on the photocatalytic CO_2 reduction over CPO-27-Mg/TiO_2 nanocomposites was also investigated and the results were shown in Fig. 5b. It shows that the introduction of CPO-27-Mg can increase the photocatalytic conversion of CO_2. An optimum amount of CPO-27-Mg was found to be 39.3%, which exhibits the highest conversion of CO_2 with 40.9 μmol g^{-1} of CO and 23.5 μmol g^{-1} of CH_4 produced in 10 h. A further increase in the CPO-27-Mg amount results in a decrease in the photocatalytic activity, which is likely due to a shading effect by the heavy loading of CPO-27-Mg.

CPO-27-Mg/TiO_2 is stable during the photocatalytic reaction as confirmed from the similar XRD patterns between the fresh and used CPO-27-Mg/TiO_2 (Supporting Fig. S6). The cycling results also showed that there was no obvious loss of the photocatalytic activity over CPO-27-Mg/TiO_2 after three runs reaction (Fig. 5c), another evidence for that the composition and structure of the photocatalyst was well preserved during the reaction.

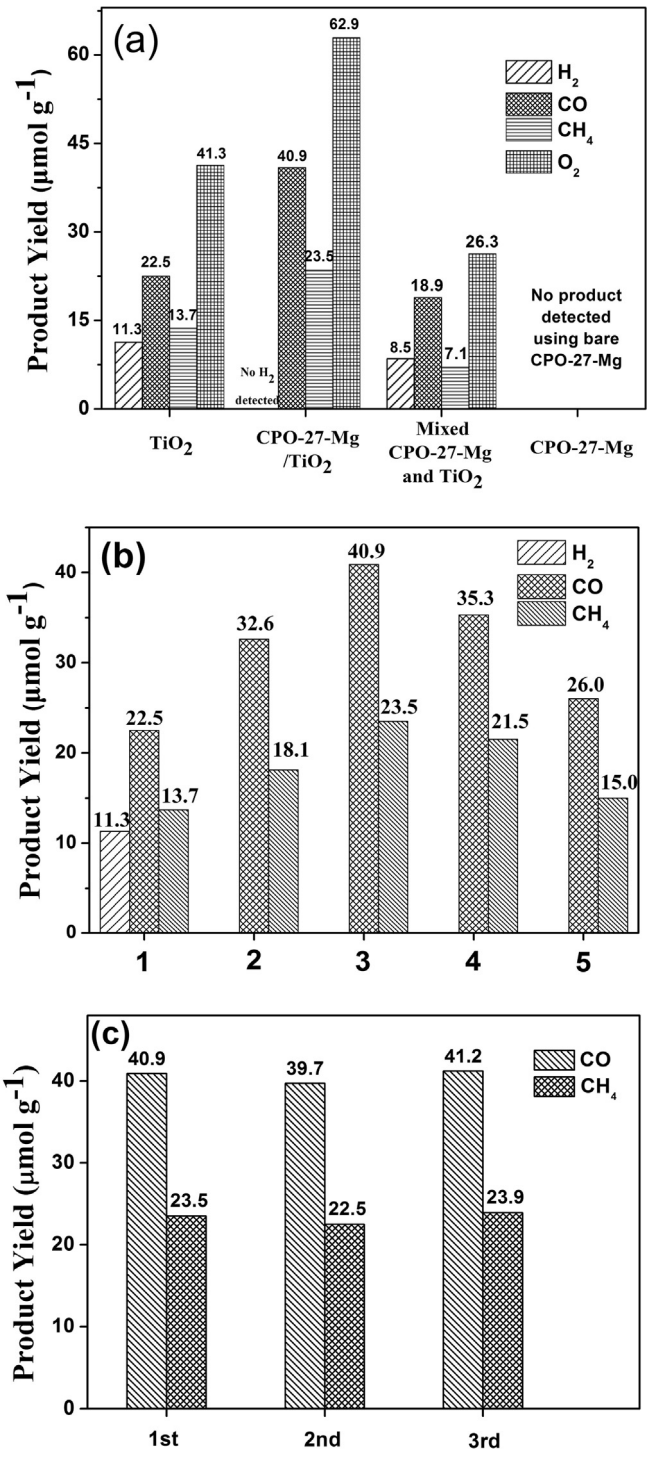

Fig. 5. (a) Yield of H_2, CO, CH_4 and O_2 over irradiated CPO-27-Mg/TiO_2 nanocomposite, TiO_2 nanospheres, CPO-27-Mg for 10 h. (b) Yield of CO, CH_4 and H_2 after irradiated for 10 h over CPO-27-Mg/TiO_2 nanocomposite with different amount of CPO-27-Mg (1) 0, (2) 26.1%, (3) 39.3%, (4) 57.2% and (5) 68.7%. (c) Yield of CO and CH_4 over irradiated CPO-27-Mg/TiO_2 in cycling runs.

4. Conclusions

In summary, CPO-27-Mg/TiO_2 composite was successfully obtained via a hydrothermal in situ growth method. The CPO-27-Mg/TiO_2 composite showed enhanced photocatalytic performance for CO_2 reduction due to its high adsorption capacity toward CO_2 and the existence of open alkaline metal sites in CPO-27-Mg. The in-situ hydrothermal method for the preparation of CPO-27-Mg/TiO_2 composites ensures that there is strong interaction between CPO-27-Mg and TiO_2, which makes CPO-27-Mg and TiO_2 work synergistically. This work provides an effective method in direct constructing a MOF/semiconductor nanocomposite. It also highlights the promising prospect of incorporating MOFs with open alkaline metal sites into semiconductors for artificial CO_2 photosynthesis.

Acknowledgements

This work was supported by 973 Program (2014CB239303), NSFC (21273035), Specialized Research Fund for the Doctoral Program of Higher Education (20123514110002) and Independent Research Project of State Key Laboratory of Photocatalysis on Energy and Environment (No. 2014A03). Z. Li thanks the Award Program for Minjiang Scholar Professorship for financial support.

Appendix A. Supplementary data

Supplementary data associated with this article can be found, in the online version, at http://dx.doi.org/10.1016/j.apcatb.2015.10.037.

References

[1] W. Wang, M.O. Tade, Z. Shao, Chem. Soc. Rev. 44 (2015) 5371–5408.
[2] P. Lanzafame, G. Centi, S. Perathoner, Chem. Soc. Rev. 43 (2014) 7562–7580.
[3] W. Tu, Y. Zhou, Z. Zou, Adv. Mater. 26 (2014) 4607–4626.
[4] G. Qin, Y. Zhang, X. Ke, X. Tong, Z. Sun, M. Liang, S. Xue, Appl. Catal. B 129 (2013) 599–605.
[5] N. Linares, A.M. Silvestre-Albero, E. Serrano, J. Silvestre-Albero, J. Garcia-Martinez, Chem. Soc. Rev. 43 (2014) 7681–7717.
[6] J. Ronge, T. Bosserez, D. Martel, C. Nervi, L. Boarino, F. Taulelle, G. Decher, S. Bordiga, J.A. Martens, Chem. Soc. Rev. 43 (2014) 7963–7981.
[7] H. Chen, C.E. Nanayakkara, V.H. Grassian, Chem. Rev. 112 (2012) 5919–5948.
[8] M. Anpo, H. Yamashita, K. Ikeue, Y. Fujii, S.G. Zhang, Y. Ichihashi, D.R. Park, Y. Suzuki, K. Koyano, T. Tatsumi, Catal. Today 44 (1998) 327–332.
[9] H. Yamashita, Y. Fujii, Y. Ichihashi, S.G. Zhang, K. Ikeue, D.R. Park, K. Koyano, T. Tatsumi, M. Anpo, Catal. Today 45 (1998) 221–227.
[10] R.B. Getman, Y.S. Bae, C.E. Wilmer, R.Q. Snurr, Chem. Rev. 112 (2012) 703–723.
[11] Y. Zhao, M. Seredych, Q. Zhong, T.J. Bandosz, ACS Appl. Mater. Interfaces 5 (2013) 4951–4959.
[12] S. Qiu, M. Xue, G. Zhu, Chem. Soc. Rev. 43 (2014) 6116–6140.
[13] J.R. Li, J. Sculley, H.C. Zhou, Chem. Rev. 112 (2012) 869–932.
[14] Y. Mao, J. Li, W. Cao, Y. Ying, L. Sun, X. Peng, ACS Appl. Mater. Interfaces 6 (2014) 4473–4479.
[15] Y. Cui, Y. Yue, G. Qian, B. Chen, Chem. Rev. 112 (2012) 1126–1162.
[16] Z. Hu, B.J. Deibert, J. Li, Chem. Soc. Rev. 43 (2014) 5815–5840.
[17] N. Ahmad, H.A. Younus, A.H. Chughtai, F. Verpoort, Chem. Soc. Rev. 44 (2015) 9–25.
[18] P. Horcajada, R. Gref, T. Baati, P.K. Allan, G. Maurin, P. Couvreur, G. Ferey, R.E. Morris, C. Serre, Chem. Rev. 112 (2012) 1232–1268.
[19] Z.J. Lin, J. Lu, M. Hong, R. Cao, Chem. Soc. Rev. 43 (2014) 5867–5895.
[20] W. Zhu, P. Liu, S. Xiao, W. Wang, D. Zhang, H. Li, Appl. Catal. B 172 (2015) 46–51.
[21] D. Sun, L. Ye, Z. Li, Appl. Catal. B 164 (2015) 428–432.
[22] D. Britt, H. Furukawa, B. Wang, T.G. Glover, O.M. Yaghi, Proc. Natl. Acad. Sci. U. S. A. 106 (2009) 20637–20640.
[23] K. Sumida, D.L. Rogow, J.A. Mason, T.M. McDonald, E.D. Bloch, Z.R. Herm, T.H. Bae, J.R. Long, Chem. Rev. 112 (2012) 724–781.
[24] Y. Fu, D. Sun, Y. Chen, R. Huang, Z. Ding, X. Fu, Z. Li, Angew. Chem. Int. Ed. 51 (2012) 3364–3367.
[25] D. Wang, R. Huang, W. Liu, D. Sun, Z. Li, ACS Catal. 4 (2014) 4254–4260.
[26] D. Sun, Y. Fu, W. Liu, L. Ye, D. Wang, L. Yang, X. Fu, Z. Li, Chem. Eur. J. 19 (2013) 14279–14285.
[27] R. Li, J. Hu, M. Deng, H. Wang, X. Wang, Y. Hu, H.L. Jiang, J. Jiang, Q. Zhang, Y. Xie, Y. Xiong, Adv. Mater. 26 (2014) 4783–4788.
[28] Q. Liu, Z.-X. Low, L. Li, A. Razmjou, K. Wang, J. Yao, H. Wang, J. Mater. Chem. A 1 (2013) 11563–11567.
[29] P. Valvekens, M. Vandichel, M. Waroquier, V. Van Speybroeck, D. De Vos, J. Catal. 317 (2014) 1–10.
[30] S.R. Caskey, A.G. Wong-Foy, A.J. Matzger, J. Am. Chem. Soc. 130 (2008) 10870–10871.
[31] Z. Bao, L. Yu, Q. Ren, X. Lu, S. Deng, J. Colloid Interface Sci. 353 (2011) 549–556.
[32] W. Liu, J. Cai, Z. Ding, Z. Li, Appl. Catal. B 174 (2015) 421–426.
[33] P.D.C. Dietzel, R. Blom, H. Fjellvåg, Eur. J. Inorg. Chem. 23 (2008) 3624–3632.
[34] F. Zasada, W. Piskorz, J. Gryboś, Z. Sojka, J. Phys. Chem. C 118 (2014) 8971–8981.

[35] X. Meng, S. Ouyang, T. Kako, P. Li, Q. Yu, T. Wang, J. Ye, Chem. Commun. 50 (2014) 11517–11519.
[36] N. Hollingsworth, S.F.R. Taylor, M.T. Galante, J. Jacquemin, C. Longo, K.B. Holt, N.H. Leeuw, C. Hardacre, Angew. Chem. Int. Ed. 54 (2015) 1–6.
[37] E. Amouyal, P. Koffi, J. Photochem. 29 (1985) 227–242.
[38] G. Zhang, W. Zhang, D. Minakata, Y. Chen, J. Crittenden, P. Wang, Int. J. Hydrogen Energy 38 (2013) 11727–11736.